

U–Pb and Lu–Hf isotopes in baddeleyite and zircon megacrysts from the Mbuji-Mayi kimberlite: constraints on the subcontinental mantle

Urs Schärer ^{a,*}, Fernando Corfu ^b, Daniel Demaiffe ^c

^a *Laboratoire de Géochronologie, Université Paris 7 and IPG–Paris, 2, Place Jussieu, F-75251, Paris Cedex 05, France*

^b *Department of Geology, Royal Ontario Museum, 100 Queen's Park, Toronto, Ontario, M5S 2C6, Canada*

^c *Laboratoire de Géochimie Isotopique (CP160/02), Université Libre de Bruxelles, Av. F.-D. Roosevelt 50, B-1050, Bruxelles, Belgium*

Received 31 January 1997; accepted 16 July 1997

Abstract

Megacrysts of baddeleyite (ZrO₂) and zircon (ZrSiO₄) from the diamond-bearing Mbuji–Mayi kimberlite were analyzed to determine their age, origin, and mantle source characteristics. Two of the five baddeleyites studied show 90° twins on the 0.05–0.2 mm scale suggesting formation at pressures ≥ 4.5 GPa, while zircon reveals a mosaic-like structure, indicative of a sudden pressure release. The 45 U–Pb analyses define an array that intercepts the concordia curve at 69.8 ± 0.5 (2 σ) and 2528 ± 452 Ma. Initial epsilon-Hf values for an age of 70 Ma are +8.4 and +8.1 for zircon and +5.1, +6.0, +6.2, +6.5, +10.2 for baddeleyite. Average Zr/Hf ratios in both minerals are almost a factor two higher than those of primitive mantle, MORB or continental crust. Baddeleyites have uranium concentrations that are exceptionally high for mantle-derived grains (780–2050 ppm). Taken together, the data indicate that zircon and baddeleyite crystallized coevally at 70 Ma in mantle reservoirs that experienced different time-integrated LILE-fractionation histories. Some limited secondary enrichment of strongly depleted mantle may have contributed to the distinct range of Hf signatures. Small amounts (< 5%) of 2.5 Ga old radiogenic Pb detected in both minerals are probably inherited from pre-existing crystals in the mantle, and high Zr/Hf ratios most likely reflect very small degrees of lherzolite melting, possibly in association with mantle metasomatism by carbonate-rich fluids. Formation of the zircon and baddeleyite megacrysts can be explained either by pre-kimberlite crystallization from different magmas or subsolidus reaction during subduction of differentiated material such as oceanic crust (+ sediments?). This latter interpretation would be in agreement with the fact that inclusions in Mbuji-Mayi diamonds, and nodules in the kimberlite are dominantly eclogitic in nature. To produce the kimberlite, and to concentrate the megacrysts in a single pipe, subsequent melting of intermingled mantle domains seems the most plausible mechanism. Moreover, formation and residence times of the evolving kimberlite magmas must have been long enough to allow extraction, re-crystallization and beginning resorption of zircon and baddeleyite. © 1997 Elsevier Science B.V.

Keywords: Kimberlites; Geochronology; U–Pb/Hf; Subcontinental mantle; Zircon; Baddeleyite

* Corresponding author. Tel.: +33 (1) 4427 2820; fax: +33 (01) 4427 8148/3373; e-mail: scharer@ipgp.jussieu.fr

1. Introduction

Rocks and minerals brought to the surface by kimberlite magmas are a key to studying of both the chemical composition and time-integrated evolution of subcontinental mantle. Megacrysts of zircon, baddeleyite, rutile, ilmenite, as well as inclusions in diamonds are of particular interest for this purpose, because they may have been derived from mantle reservoirs that experienced different episodes of continental growth and hence, mantle depletion. Uranium-bearing minerals such as zircon and baddeleyite allow precise dating of the megacrysts, and high Hf (≈ 1.4 Wt.%) in these minerals can be used for isotope tracing, to potentially establish time-space cross-sections through the continental lithosphere underneath regions of kimberlite magmatism.

For this reason, we performed 45 U–Pb analyses and 7 Lu–Hf isotope determinations on two zircon and five baddeleyite megacrysts, complemented by

optical microscopy, electron microscopy, and electron micro-probe analyses to investigate grain characteristics. Our zircon and baddeleyite megacrysts originate from the same kimberlite pipe in the Mbuji-Mayi kimberlite field in Central Africa, and because these grains occur together with diamonds, knowledge on their formation can contribute to the understanding on the origin of diamonds.

2. Geological and mineralogical outline

Fig. 1 shows the location of the Mbuji-Mayi kimberlite field and a schematic cross-section through the pipe. The field consists of two clusters of pipes: the northern group of ten kimberlite bodies (Mbuji-Mayi itself) that form elliptic basins along an E–W-striking crustal fissure in the Kasai Craton (e.g., Fieremans, 1977; Demaiffe and Fieremans, 1981;

SCHEMATIC STRATIGRAPHIC SEQUENCE INTRUDED BY THE MBUJI-MAYI KIMBERLITE PIPES

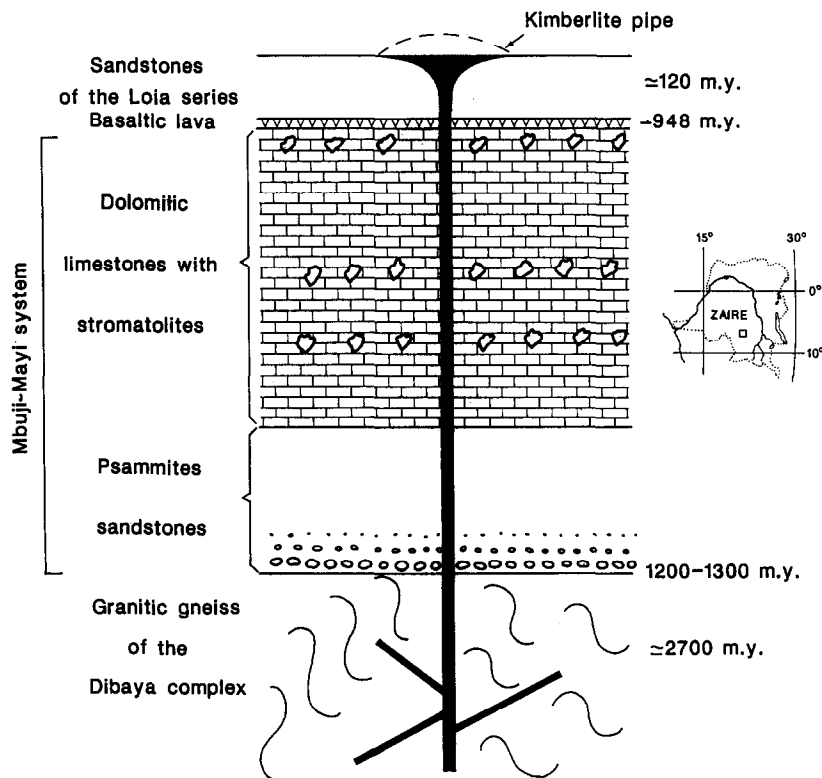


Fig. 1. Schematic cross-section through the Mbuji-Mayi kimberlite pipe (Central Africa).

Demaiffe et al., 1991), and a southern group of five pipes (Tshibua). The Mbuji-Mayi field is one of the largest diamond-producing centres of the world with about 12×10^6 carats of diamonds extracted per year. The pipes were emplaced into approximately 2.7 Ga old granitic gneisses of the Dibaya complex (Delhal et al., 1975), and 1.3–0.95 Ga old Mbuji-Mayi sedimentary series. These two units were covered around 0.95 Ga by basaltic lavas, and by much younger, Cretaceous sandstones (≈ 120 Ma), which define a maximum age for kimberlite emplacement.

The Mbuji-Mayi kimberlites are described as xeno-tuff-breccias containing eclogite nodules (Elfadili et al., 1995), megacrysts of pyrope, clinopyroxene and Mg-ilmenite ('discrete nodule association'; Nixon and Boyd, 1973), and porphyritic rounded nodules ('primary kimberlite' or 'autoliths') as well as fragments of country rocks. Two generations of olivine in the rounded nodules are replaced by phlogopite and calcite (Fieremans and Ottenburgs, 1979a), whereas the matrix is composed of very fine phyllitic and calcite grains, with accessory magnetite, rutile and apatite.

The classical megacryst suite at Mbuji-Mayi (Mvuemba, 1980) is composed of (1) clinopyroxenes that are either omphacitic (Na- and Al-rich), comparable to eclogite pyroxenes, or Cr-poor diopsides (0.5–0.8% Cr₂O₃), (2) garnet megacrysts that are either Cr-rich pyrope (up to 7% Cr₂O₃) or Ca-rich (Cr-poor) eclogitic garnets, and (3) Mg- and Cr-rich ilmenite (10–15% MgO; 1.5–4% Cr₂O₃). Beside this 'classical' megacryst suite, the Mbuji-Mayi kimberlites contain zircon and baddeleyite megacrysts (Fieremans and Ottenburgs, 1979b) and grains of silicate–rutile intergrowth (Ottenburgs and Fieremans, 1979). The average size of the zircons and baddeleyite is 0.5 cm but crystals as large as 2 cm have been reported. They are round to subround with some zircon grains showing a thin white coating of baddeleyite.

3. Previous isotope data

3.1. Ages

Using TIMS, Davis (1977) reported a $^{206}\text{Pb}/^{238}\text{U}$ date of about 71 Ma for a zircon of the Mbuji-Mayi

kimberlite; no $^{207}\text{Pb}/^{235}\text{U}$ date was given, probably due to very low U and high initial common Pb. Another date of 628 ± 12 (2σ) Ma was obtained by SIMS (SHRIMP) U–Pb dating on a 0.1 mm large zircon inclusion in a diamond, extracted from one of the Mbuji-Mayi kimberlites (Kinny and Meyer, 1994). However, due to its unusual age and high U-concentrations (up to 650 ppm) this small zircon inclusion was interpreted to be distinct from the cm-size low-U megacrystic zircons from Mbuji-Mayi kimberlites.

3.2. Isotope tracing

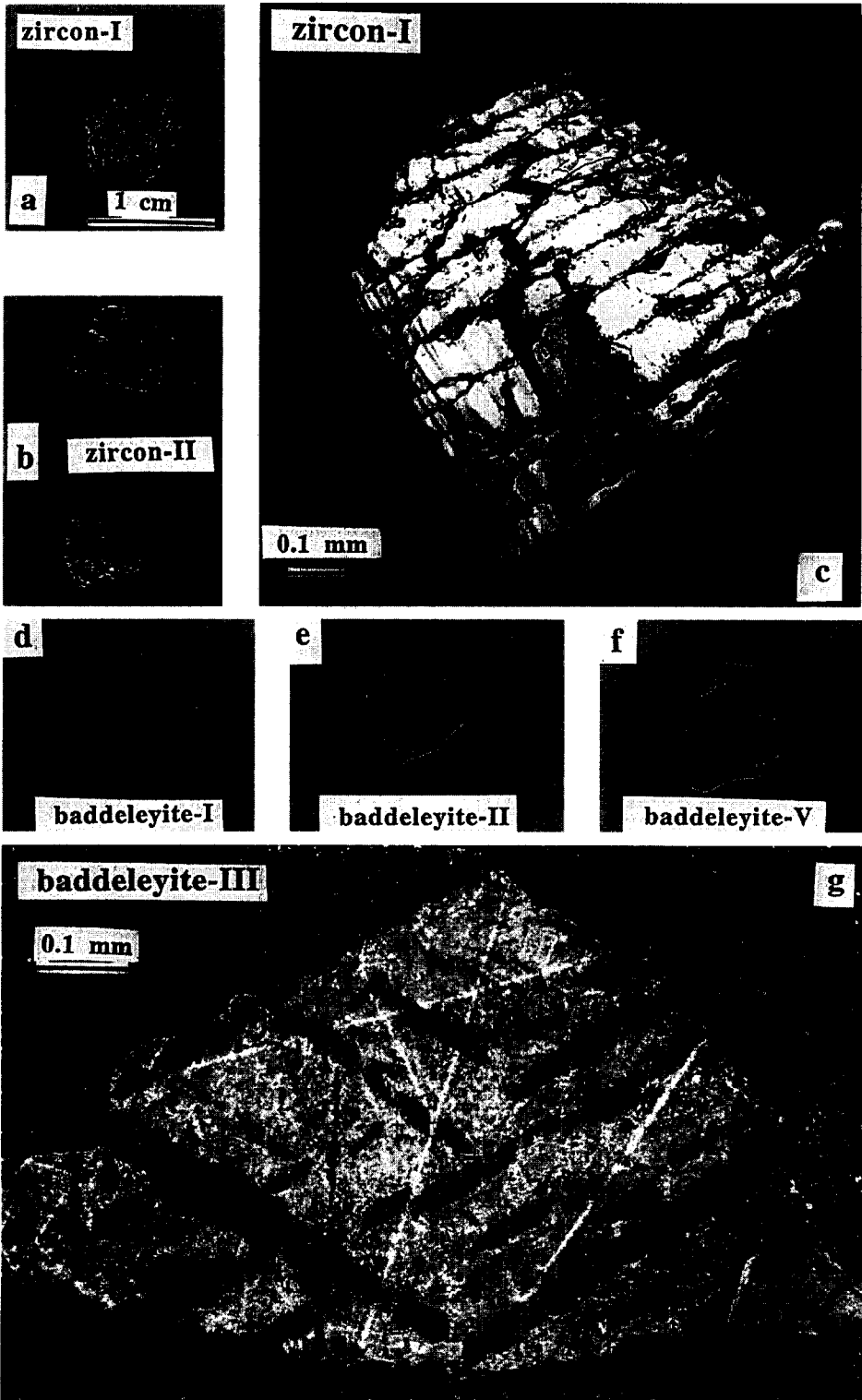
Sr–Nd–Pb isotope data on primary kimberlite nodules (autoliths), bluegrounds, carbonate inclusions and diopside megacrysts suggest that crustal contamination of the kimberlite magma was very small. Initial (70 Ma) $^{87}\text{Sr}/^{86}\text{Sr}$ values (I_{sr}) lie between 0.7040 and 0.7045, initial epsilon-Nd values ($\epsilon_{70\text{Ma}}^{\text{Nd}}$) +2 and +6, and $^{207}\text{Pb}/^{204}\text{Pb}$ 15.554 and 15.590 (Demaiffe and Fieremans, 1981; Fieremans et al., 1984; Weis and Demaiffe, 1985). Pb isotope ratios, and possibly some of the lower $\epsilon_{70\text{Ma}}^{\text{Nd}}$ values yield evidence for crustal components.

Nitrogen and carbon isotope data of Mbuji-Mayi diamonds (Javoy et al., 1984) indicate a complex crystallization history, occurring in deep-seated reservoirs which yield $\delta^{15}\text{N}$ values between -11.2 and $+6.0\%$. For $\delta^{13}\text{C}$, a range between -11.8 and -4.6% was observed, for large-cubic and small-oc-tahedral diamonds, as well as for kimberlite carbonates.

4. Analytical procedures

4.1. U–Pb

The zircon and baddeleyite megacrysts were split into two roughly equal pieces. One of these pieces was then broken into a large series of 0.1 to 2 mm fragments, in an agate-mortar under alcohol. A few analyses were carried out on crystal powders produced from some fragments. Zircon was dissolved for one week in HF 50% at 220°C in Teflon pressure capsules (Krogh, 1973). Initially, baddeleyite analyses were carried out in the same way with a dissolu-



tion time of four days; later they were dissolved with HF 50% over two days in Teflon beakers, on a hot plate at 200°C. All samples were spiked using a mixed ^{205}Pb – ^{233}U – ^{235}U isotope tracer, added prior to dissolution. ID and IC measurements were carried out using either a VG-Sector mass-spectrometer in Montreal, or Thomson 206 and 206C instruments in Paris. On all three machines, single Faraday or secondary electron collectors were used. Mass-discrimination was controlled by regular measurements of the NBS-981 common Pb standard. Over the period of analyses, discrimination was $0.1 \pm 0.05\%$ /amu for both U and Pb isotope ratios. Pb and U were loaded simultaneously with silicagel and phosphoric acid on a single Re-filament and run at 1350–1450°C for Pb^+ , and at 1450–1550°C for UO_2^+ (Schärer and Gower, 1988). Major and trace element analyses were performed on a Cameca SX-50 electron microprobe. Secondary electron (SE) and cathodoluminescence images (CL) were produced on a Jeol JSM-840A scanning electron microscope (both at University of Paris 7).

4.2. Lu–Hf

For each analysis a 1 to 3 mg fragment of zircon or baddeleyite was dissolved. After evaporation of HF, the residue was again dissolved overnight in 3.1 N HCl, then a 10% aliquot was spiked with a ^{176}Lu – ^{180}Hf tracer and the remaining solution was used for IC measurements. Separation of Lu and Hf, loading and measurements were carried out at Toronto (Corfu and Noble, 1992). Replicate measurements of the JMC 475-2 Hf standard in the period of the study yield $^{176}\text{Hf}/^{177}\text{Hf} = 0.282142 \pm 21 (2\sigma)$.

5. The zircon and baddeleyite megacrysts

Photos of 0.6 to 1.1 cm sized zircon and baddeleyite megacrysts are shown in Fig. 2. Despite round-

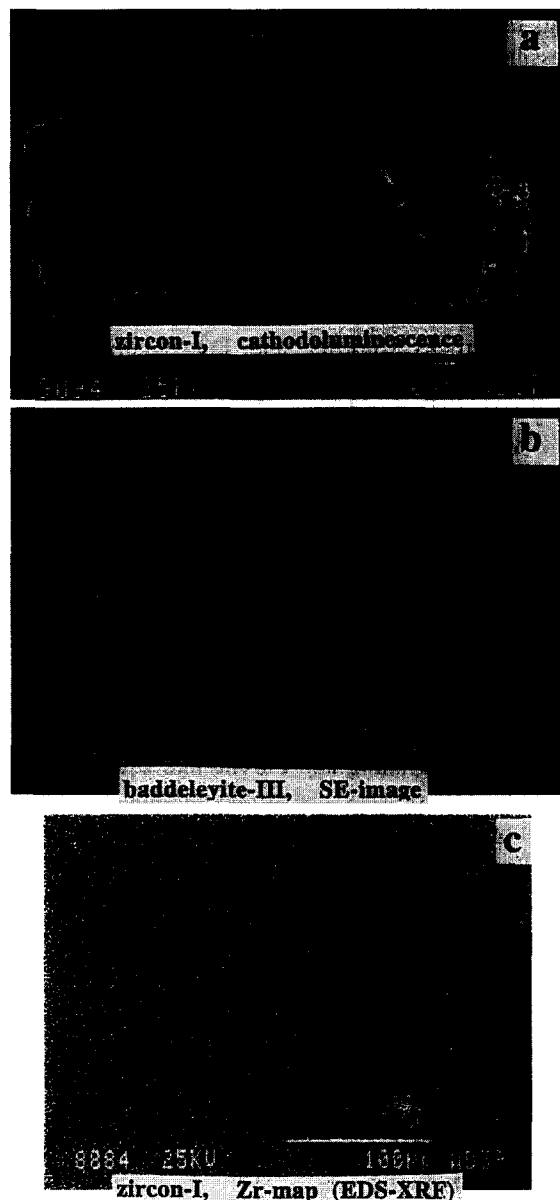


Fig. 3. (a) Cathodoluminescence image of an about 1.5 mm large zircon fragment. (b) SE-image of twins in baddeleyite-III. (c) Distribution of Zr in zircon as revealed by mapping its characteristic X-waves.

Fig. 2. (a, b) The two zircon megacrysts analyzed, with zircon-II broken in two halves. (c) Mosaic-like structure of zircon-I distinguished under polarized light, where the dark domains correspond to the extinction position under crossed Nicols. (d–f) Three of the baddeleyite megacrysts analyzed (same scale as the zircons). (g) HF-etched surface of baddeleyite-III showing orthogonal twinning indicative of pressures ≥ 4.5 GPa (the 120° angle is caused by the oblique sectioning of the grain).

ing, recognition of original crystal surfaces is still possible, similar to that of baddeleyites in the *Île Bizard* alnöite (Heaman and LeCheminant, 1993). The subrounded shapes may indicate incipient resorption of the grains in the kimberlite magma or abrasion during ascent. Examined under polarized light, the two zircon grains reveal a mosaic-like structure (Fig. 2c), which could be a stress-produced feature affecting the megacrysts at great depth (> 120 km). Mosaicism is a well known phenomenon in shocked rocks (Stöffler and Langenhorst, 1994), where high peak-shock pressures are followed by very fast pressure release.

Two of the five baddeleyite grains show microscopically visible 90° twins on the 0.05–0.20 mm scale. A leached surface (dilute HF) of a baddeleyite twins is shown in Fig. 2g. Such twinning has been observed in experimental studies of the ZrO₂-system (Kudoh et al., 1989) where twins are stress-induced at pressures ≥ 4.5 GPa. The apparent octahedral shape of the baddeleyite is consistent with an original tetragonal symmetry. Although we have not examined the zircon and baddeleyite structures in more detail, both twinning and mosaic-like structure may be indicative of very fast decompression in the ascending kimberlite.

The zircon and baddeleyite megacrysts were also analyzed with the electron micro-probe and the scanning electron microscope (Fig. 3). The two minerals, including both twin-domains of baddeleyite and the

mosaic-like structured zircons, show very homogeneous chemical composition (Table 1). Intergrowth or overgrowth phases could not be detected neither by cathodoluminescence on zircon, nor by electron imaging of either minerals, nor by mapping of specific elements such as Zr in zircon. Zircon displays a very diffuse compositional banding (Fig. 3a) but lacks the pronounced zoning as is common in accessory crustal zircons of magmatic or metamorphic origin.

Baddeleyites contain 0.8 wt.% TiO₂ and trace amounts (≈ 100 ppm) of Ca, Co, Cr and Mg (Table 1). Zircon is characterized by traces of Ni, Co, Cr and Ti (0.2 wt.% oxides). An important feature is the strong depletion of Hf in zircon (Zr/Hf = 58) relative to zircons of continental crust, primitive mantle and N-MORB (Zr/Hf: 33–36; e.g., Murali et al., 1983; Jochum et al., 1986; Heaman et al., 1990). Exceptionally high Zr/Hf ratios have also been reported for whole-rock samples of the Nyiragongo nephelinite (Dupuy et al., 1992), for zircons extracted from continental rift carbonatites and nepheline syenites (Heaman et al., 1990), as well as for zircon from the Jwaneng kimberlite (Kinny et al., 1989). Zircons from several other kimberlites display a broad variation in Zr/Hf ratios (Kresten et al., 1975). For baddeleyite, the measured Zr/Hf ratios of 65 lie in the range reported for terrestrial and lunar grains (Scatena-Wachel and Jones, 1984; Heaman and LeCheminant, 1993).

Table 1
Average chemical composition of zircon and baddeleyite megacrysts from the Mbuji-Mayi kimberlite

Wt.%	Zircon	Baddeleyite			
ZrO ₂	66.5	97.1			
SiO ₂	33.0				
HfO ₂	0.9	1.3			
TiO ₂		0.8			
Σ (Ni,Co,Cr,Ti-oxides)	0.2				
Σ (Ca,Co,Cr,Mg-oxides)		0.4			
	100.6	99.6			
	Mbuji-Mayi Zircons	Baddeleyites	Crustal zircons	Primitive mantle	N-MORB
Zr/Hf	58	65	33–36	35	36
Hf (ppm)	7600	11000	10000–12000		

Average values from 7 to 15 individual electron probe micro-analyses (EPMA) performed on a Cameca SX-50 instrument.

6. U–Pb dating results

6.1. General considerations

Table 2 lists the U–Pb isotopic data, Figs. 4 and 5 show the corresponding concordia diagrams, and Fig. 6 illustrates observed variations of initial common Pb in zircon and baddeleyite. All crystal fragments were carefully examined under the binocular microscope, to select only perfectly transparent and homogeneous pieces, free of inclusions and cracks. To avoid potentially altered rims, only the interior of the megacrysts were used for analysis, and most fragments were additionally abraded prior to final selection (Krogh, 1982).

All U–Pb analyses are corrected for initial common Pb using values of 18.01 for $^{206}\text{Pb}/^{204}\text{Pb}$ (α), 15.47 for $^{207}\text{Pb}/^{204}\text{Pb}$ (β), and 37.71 for $^{208}\text{Pb}/^{204}\text{Pb}$ (γ), which correspond to a 70 Ma model-mantle source (Zartman and Doe, 1981). No cogenetic low- $^{238}\text{U}/^{204}\text{Pb}$ (μ) mineral phases are available in the kimberlite to independently determine initial Pb isotopic compositions. This correction has only moderate influence on analyses with high α -values but cause significant uncertainties for analyses with α -values below about 500. To include this uncertainty, we propagated a relative error of $\pm 5\%$ on $^{207}\text{Pb}/^{206}\text{Pb}$ for initial Pb, corresponding

to the entire range of $^{207}\text{Pb}/^{206}\text{Pb}$ measured for Atlantic and Pacific MORB sources (e.g., Ito et al., 1988). Corrections and errors given in the concordia diagrams therefore account for possible variations of initial Pb isotopic compositions in Cretaceous mantle.

6.2. Zircon

Eleven 0.271 to 2.24 mg fragments were analyzed for *zircon megacryst-I*. Uranium abundances range between 48 and 81 ppm, with one large fragment having 131 ppm. Radiogenic Pb is less than 1 ppm, except for one fragment that has 1.51 ppm. Measured common Pb exceeds the level of Pb introduced during the analytical procedure by a factor of up to 65 (total blank: 10–15 pg). This shows that measured common Pb is essentially initial Pb, incorporated by the grains during growth or re-crystallization. The data of *megacryst-I* define a tight cluster in the concordia diagram of Fig. 4a, yielding U–Pb ages between 71.3 and 79.2 Ma, and $^{207}\text{Pb}/^{206}\text{Pb}$ ages between 218 and 283.

From *zircon megacryst-II* eight fragments weighing between 1.02 and 0.19 mg define U–Pb ages between 70.5 and 85.6 Ma, and $^{207}\text{Pb}/^{235}\text{U}$ ages between 144 and 382 Ma, plotting discordantly in the concordia diagram of Fig. 4b. Uranium abundances are significantly lower than in *megacryst-I*, ranging from 7.4 to 37 ppm, and radiogenic Pb is less than 0.79 ppm. Initial common Pb is equal or slightly higher than in the first zircon, reaching 1 ppm in one analysis (Nr. 14, Table 2; Fig. 6).

6.3. Baddeleyite

Five fragments of *baddeleyite-I* yield U–Pb ages between 69.6 and 75.7 Ma, and $^{207}\text{Pb}/^{206}\text{Pb}$ ages lie between 158 and 184. In the concordia diagram of Fig. 5a, the fragments (weighing 0.29 to 1.56 mg) scatter in a narrow range plotting roughly parallel to the concordia curve. High U (778 to 2046 ppm) correlates with equally varying concentrations of initial common Pb that ranges between 0.3 and 4 ppm (Fig. 6)

Five analyses (0.11 to 1.21 mg) of *baddeleyite-II* (Fig. 5b) yield slightly discordant ages (Fig. 5b) that are identical within analytical uncertainty, yielding

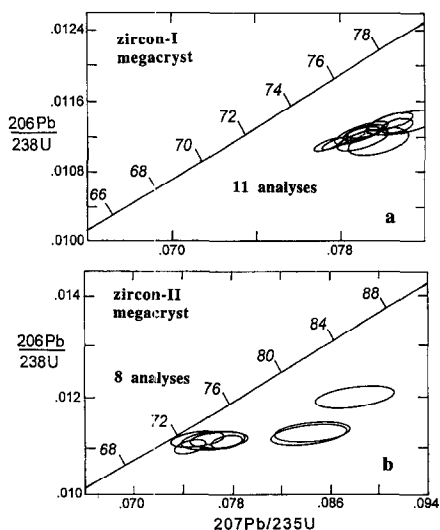


Fig. 4. Concordia diagram for U–Pb analyses of fractions from the two zircon megacrysts.

Table 2
U–Pb analytical results for zircon and baddeleyite megacrysts from the Mbuji-Mayi kimberlite

Sample ^a	Weight (mg)		Element abundances (ppm) ^b		²⁰⁶ Pb/ ²⁰⁴ Pb measured ^d	Radiogenic Pb in atomic % ^e		Atomic ratios ^e		Apparent ages in Ma				
	U	Pb _{ad}	Pb _{ad}	Pb _{con} ^c		²⁰⁶ Pb/ ²³⁸ U	²⁰⁷ Pb/ ²³⁵ U	²⁰⁶ Pb/ ²³⁸ U	²⁰⁷ Pb/ ²³⁵ U	²⁰⁶ Pb/ ²³⁸ U	²⁰⁷ Pb/ ²³⁵ U	²⁰⁷ Pb/ ²⁰⁶ Pb		
Zircons														
Megacryst-I														
(1) 1 fragment**	0.284	62	0.71	28	469	84.5	4.3	11.2	0.01113	0.07753	0.05051	71.4	75.8	218
(2) 2 fragments**	0.584	64	0.72	323	99.2	85.4	4.4	10.2	0.01113	0.07972	0.05195	71.4	77.9	283
(3) powder	0.271	59	0.66	70	179	86.2	4.4	9.4	0.01114	0.07897	0.05143	71.4	77.2	260
(4) 1 large fragm.**	0.867	131	1.51	73	1109	82.9	4.2	13.9	0.01112	0.07767	0.05067	71.3	76.0	226
(5) 1 fragment*	0.466	48	0.54	92	191	86.2	4.4	9.4	0.01134	0.08013	0.05126	72.7	78.3	252
(6) 2 fragments	0.494	81	0.93	102	297	84.1	4.3	11.6	0.01127	0.07916	0.05095	72.2	77.4	239
(7) 4 fragments	0.674	73	0.85	160	235	83.2	4.3	12.5	0.01129	0.08044	0.05169	72.4	78.6	272
(8) 1 very large fr.*	1.710	48	0.53	88	677	86.9	4.4	8.7	0.01122	0.07852	0.05073	72.0	76.8	229
(9) 1 very large fr.*	2.240	60	0.69	1006	114	85.0	4.4	10.6	0.01137	0.08109	0.05175	72.9	79.2	274
(10) 1 fragment*	0.530	66	0.74	73	355	86.5	4.4	9.1	0.01122	0.07907	0.05111	71.9	77.3	246
(11) 4 fragments*	0.300	54	0.61	64	197	86.4	4.4	9.2	0.01120	0.07884	0.05104	71.8	77.0	243
Megacryst-II														
(12) 1 fragment**	0.190	20	0.23	33.0	99.9	85.6	4.2	10.1	0.01099	0.07457	0.04920	70.5	73.0	157
(13) 2 fragments**	0.188	30	0.34	46.6	104	85.4	4.3	10.3	0.01110	0.07742	0.05058	71.2	75.7	222
(14) 18 small fr.**	0.368	37	0.42	365	44.8	86.0	4.7	9.3	0.01124	0.08406	0.05427	72.0	82.0	382
(15) 1 large fragm.**	1.024	7.4	0.09	176	48.9	83.0	4.5	12.5	0.01133	0.08434	0.05397	72.6	82.2	370
(16) 1 large fragm.**	0.720	21	0.23	192	72.4	85.2	4.2	10.6	0.01114	0.07517	0.04893	71.4	73.6	144
(17) powder	0.289	26	0.36	235	42.5	75.6	4.0	20.4	0.01201	0.08794	0.05312	77.0	85.6	334
(18) 1 fragment	0.270	31	0.79	149	58.0	85.2	4.3	10.5	0.01113	0.07666	0.04994	71.4	75.0	192
(19) 3 fragments*	0.360	24	0.28	172	53.9	84.5	4.2	11.3	0.01114	0.07650	0.04979	71.4	74.9	195
Baddeleyites														
Megacryst-I														
(20) 5 fragments**	0.372	1821	18.3	605	795	94.1	4.6	1.3	0.01099	0.07478	0.04937	70.4	73.2	166
(21) 1 fragment	0.559	1823	18.9	1037	716	94.0	4.7	1.3	0.01131	0.07735	0.04962	72.5	75.7	177
(22) 1 fragment*	0.292	1788	18.2	446	839	94.1	4.6	1.3	0.01116	0.07587	0.04931	71.5	74.3	163
(23) 1 fragment*	1.560	778	7.71	553	1515	94.2	4.6	1.2	0.01086	0.07368	0.04922	69.6	72.2	158
(24) 1 fragment	0.720	2046	20.9	3145	346	94.1	4.7	1.2	0.01116	0.07657	0.04977	71.5	74.9	184

Megacryst-II														
(25) 4 fragments **	0.110	1283	13.0	64	1561	94.3	4.7	1.0	0.01113	0.07646	0.04983	71.4	74.8	187
(26) 2 fragments	1.205	1319	13.4	509	2198	94.2	4.7	1.1	0.01111	0.07622	0.04975	71.2	74.6	183
(27) 1 fragment *	0.940	385	3.9	155	1647	94.2	4.7	1.1	0.01114	0.07611	0.04954	71.4	74.5	174
(28) 10 small fr. **	0.078	1250	12.7	33.1	2086	94.3	4.7	1.0	0.01110	0.07629	0.04985	71.2	74.6	188
(29) 6 fragments *	0.108	1274	12.9	42.7	2290	94.2	4.7	1.1	0.01112	0.07631	0.04979	71.3	74.7	185
Megacryst-III														
(30) 4 fragments **	0.306	1332	13.4	870	345	94.1	4.7	1.2	0.01104	0.07625	0.05008	70.8	74.6	199
(31) 11 small fr. **	0.249	954	9.7	523	336	94.1	4.7	1.2	0.01107	0.07638	0.05002	71.0	74.7	196
(32) 1 fragment *	0.670	1167	11.8	181	3039	94.3	4.6	1.1	0.01111	0.07495	0.04892	71.2	73.4	144
(33) 1 fragment *	0.327	1434	14.7	1087	322	94.0	4.7	1.3	0.01122	0.07783	0.05032	71.9	76.1	210
(34) 1 fragment	0.780	436	4.4	214	1114	94.3	4.6	1.1	0.01099	0.07432	0.04906	70.4	72.8	151
(35) 2 fragments *	1.231	1384	14.0	2265	543	94.1	4.7	1.2	0.01110	0.07661	0.05005	71.2	75.0	197
Megacryst-IV														
(36) 1 fragment	2.138	1208	12.0	739	2414	94.3	4.6	1.1	0.01090	0.07391	0.04916	69.9	72.4	156
(37) 1 fragment	0.875	1174	11.9	397	1823	94.3	4.6	1.1	0.01109	0.07521	0.04917	71.1	73.6	156
(38) 1 fragment *	0.760	1419	14.3	371	2037	94.3	4.6	1.1	0.01106	0.07508	0.04925	70.9	73.5	160
(39) 5 small fr. **	0.155	1083	10.9	59.7	1985	94.4	4.6	1.0	0.01104	0.07445	0.04891	70.8	72.9	144
(40) 1 fragment **	0.143	1370	13.7	54.5	2529	94.3	4.6	1.1	0.01101	0.07478	0.04927	70.6	73.2	161
Megacryst-V														
(41) 1 large fragm. *	1.170	1069	10.7	397	2190	94.4	4.5	1.1	0.01097	0.07236	0.04784	70.3	70.9	91.5
(42) 1 large fragm. **	1.020	919	9.02	474	1357	94.2	4.5	1.3	0.01076	0.07089	0.04776	69.0	69.5	87.7
(43) 1 large fragm. *	1.800	1044	10.0	1697	753	94.6	4.5	0.9	0.01056	0.06903	0.04741	67.7	67.8	70.0
(44) 1 fragment *	0.780	960	9.7	238	2220	94.4	4.5	1.1	0.01112	0.07319	0.04772	71.3	71.7	85.3
(45) 1 fragment	0.420	1956	19.8	313	1849	94.3	4.5	1.2	0.01110	0.07375	0.04818	71.2	72.3	108

* Samples analyzed are small pieces (fragments) of the megacrysts. Prior and after fragment abrasion (Krogh, 1982), the individual fragments were selected under the binocular microscope, and only best quality fragments were used for dating. * = 5–15 vol.% abraded; ** = 15–30 vol.% abraded; no asterisk = not abraded.

^b Corrected for mass-discrimination, isotopic tracer contribution, 15 pg of Pb blank, 1 pg of U blank, and initial Pb (see below).

^c Total amount of common Pb (in 10⁻¹² g., corrected for mass-discrimination and isotopic tracer contribution).

^d Corrected for mass-discrimination and isotopic tracer contribution.

^e Ratios corrected for mass-discrimination, isotopic tracer contribution, 15 pg of Pb blank, 1 pg of U blank, and initial common Pb as deduced from Pb evolution models for the mantle (Zartman and Doe, 1981). Initial Pb values used are: 18,010 for ²⁰⁶Pb/²⁰⁴Pb, 15,470 for ²⁰⁷Pb/²⁰⁴Pb, and 37,710 for ²⁰⁸Pb/²⁰⁴Pb; for discussion see text. Ratios are not corrected for deficit ²⁰⁶Pb (initial disequilibrium in ²³⁰Th; Schärer, 1984); for discussion see text.

^f Decay constants from Jaffey et al. (1971) used are as recommended by IGC (Steiger and Jäger, 1977).

U–Pb ages around 74 Ma and $^{207}\text{Pb}/^{206}\text{Pb}$ ages around 185 Ma. U concentrations (385 and 1319 ppm) are slightly lower than in *baddeleyite-I* but are still very high compared to zircon, and initial common Pb is quite constant (less than 1 ppm).

Six fragments of *baddeleyite-III* (0.25 to 1.23 mg) give ages that define a narrow field in the concordia diagram of Fig. 5c, with four points being identical and two others yielding slightly younger U–Pb ages. The entire range of U–Pb ages is from 70.4 to 76.1, and $^{207}\text{Pb}/^{206}\text{Pb}$ ages lie between 144 and 210 Ma. Uranium concentrations (436 to 1434 ppm) are comparable to those in the first two baddeleyites.

Five analyses (0.14 and 2.14 mg) from *baddeleyite-IV* yield almost identical dates plotting in a narrow field in the concordia diagram of Fig. 5d. U–Pb ages lie between 70 and 74 Ma and $^{207}\text{Pb}/^{206}\text{Pb}$ ages are 144 to 161 Ma. Uranium concentrations are rather homogeneous (1083 to 1419 ppm) and initial common Pb lies below 0.5 ppm.

Compared to the four other baddeleyites, five analyses of *baddeleyite-V* define slightly younger ages being 67.8 to 72.3 Ma for U–Pb, and 70.0 to 108 Ma for $^{207}\text{Pb}/^{206}\text{Pb}$ (Fig. 5e). Uranium abundances range from 919 to 1956 ppm, and initial common Pb varies correspondingly between 0.3 and 1 ppm.

7. Lu–Hf isotope data

Abraded megacryst fragments (1 and 3 mg) were also analyzed for Lu–Hf. For *zircon-I* a duplicate analysis on a separately dissolved fragment was performed to test for reproducibility. Table 3 lists the analytical data, as well as initial epsilon-Hf values (ϵ_i^{Hf}) calculated for a crystallization age of 70 Ma. Both zircons and baddeleyites have very low Lu concentrations between 2 to 5 ppm. This makes corrections for in situ decay of ^{176}Lu very small, and $^{176}\text{Hf}/^{177}\text{Hf}$ ratios are age-invariant, i.e., measured $^{176}\text{Hf}/^{177}\text{Hf}$ are essentially the same as initial values at 70 Ma.

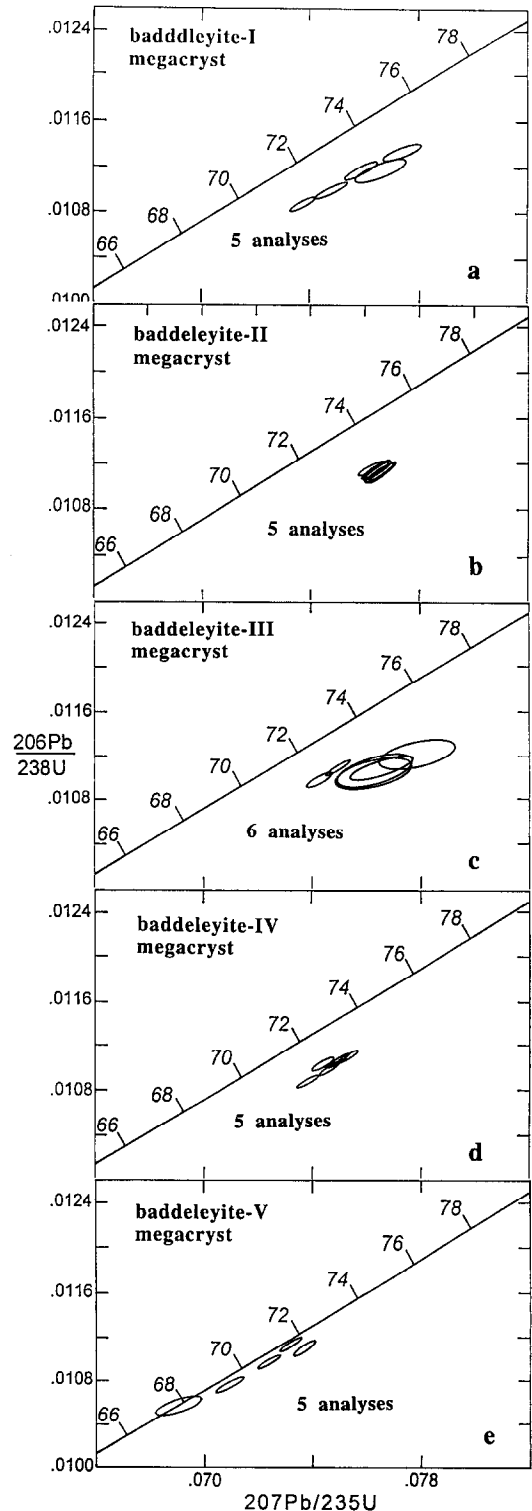


Fig. 5. Concordia diagram for U–Pb analyses of fractions from the five baddeleyite megacrysts.

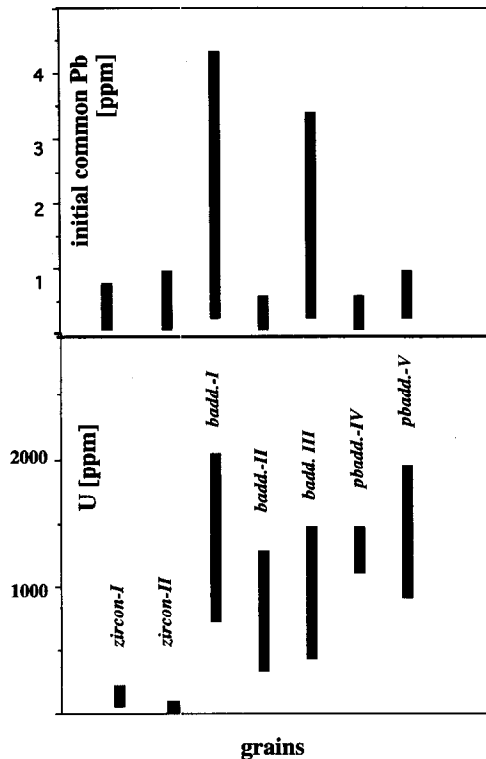


Fig. 6. U and common Pb concentrations observed for the 45 individual fractions analyzed.

Initial Hf isotope signatures of the megacrysts show differences that largely exceed analytical uncertainties. *Baddeleyite-I* yields the least radiogenic

$\varepsilon_{70 \text{ Ma}}^{\text{Hf}}$ of 5.1 ± 0.6 (2σ) followed by *baddeleyite-II*, *III*, and *V* which give $\varepsilon_{70 \text{ Ma}}^{\text{Hf}}$ of 6.2 ± 0.5 , 6.0 ± 0.5 , and 6.5 ± 0.4 , respectively. The three latter values are indistinguishable from each other. *Baddeleyite-IV* yields the most radiogenic $\varepsilon_{70 \text{ Ma}}^{\text{Hf}}$ of 10.2 ± 0.5 . The two zircon megacrysts have $\varepsilon_{70 \text{ Ma}}^{\text{Hf}}$ of 8.4 ± 0.6 and 8.1 ± 0.6 for *zircon-I* and *II*, respectively. Duplicate analysis of another fragment of *zircon-I* yields a strictly identical result (8.4 ± 0.6) which shows that different fragments of the same megacryst have identical Hf isotope signatures.

8. Age interpretation and discussion

8.1. Possible interpretations

As shown in Fig. 7a, the 45 zircon and baddeleyite U–Pb analyses define a data array for which only very few analyses plot on or close to concordia. A regression line including all data intercepts the concordia curve at 69.8 ± 0.5 (2σ) and 2528 ± 452 Ma (MSWD = 7.6). Three possibilities can explain the data set, herein called Models A to C. *Model A*: primary formation of the megacrysts is of late Palaeozoic–Mesozoic age ($^{207}\text{Pb}/^{206}\text{Pb}$ ages, Table 2) followed by large degrees of Pb-loss in very recent times (< 10 Ma). *Model B*: a thermal event at 70 Ma caused Pb-loss in ≈ 2.5 Ga old megacrysts. *Model C*: the 70 Ma age dates formation of the

Table 3

Lu–Hf analytical results for zircon and baddeleyite megacrysts from the Mbuji-Mayi kimberlite

Sample	Lu (ppm)	$^{176}\text{Lu}/^{177}\text{Hf}$	$(^{176}\text{Hf}/^{177}\text{Hf})_{\text{meas.}}$	$\varepsilon_{70 \text{ Ma}}^{\text{Hf}}$
<i>Zircon</i>				
Megacryst-I/1	4	0.0000739	0.282993 ± 17	$+8.4 \pm 0.6$
Megacryst-I/2	3	0.0000618	0.282995 ± 16	$+8.4 \pm 0.6$
Megacryst-II	3	0.0000605	0.282987 ± 18	$+8.1 \pm 0.6$
<i>Baddeleyites</i>				
Megacryst-I	4	0.0000536	0.282902 ± 13	$+5.1 \pm 0.5$
Megacryst-II	2	0.0000266	0.282931 ± 15	$+6.2 \pm 0.5$
Megacryst-III	2	0.0000263	0.282927 ± 11	$+6.0 \pm 0.4$
Megacryst-IV	2	0.0000222	0.283045 ± 15	$+10.2 \pm 0.5$
Megacryst-V	5	0.0000670	0.282940 ± 11	$+6.5 \pm 0.4$

$(^{176}\text{Hf}/^{177}\text{Hf})_{\text{meas.}}$ is normalized to $^{179}\text{Hf}/^{177}\text{Hf} = 0.7325$ (Patchett and Tatsumoto, 1980). The ^{176}Lu decay constant is $1.94 \times 10^{-11} \text{ y}^{-1}$ (Patchett, 1983), and the values used to calculate $\varepsilon_{70 \text{ Ma}}^{\text{Hf}}$ are: $(^{176}\text{Hf}/^{177}\text{Hf})_{\text{CHUR}} \text{ today} = 0.282802$ (Patchett, 1983), adopted to the JMC-475-2 Standard value of 0.282142, and $(^{176}\text{Lu}/^{177}\text{Hf})_{\text{CHUR}} = 0.334$ (Patchett, 1983), yielding $(^{176}\text{Hf}/^{177}\text{Hf})_{\text{CHUR}} = 0.282757$ for 70 Ma, and 0.281142 for 2500 Ma. Use of the recently re-determined present-day mean values for chondrites (Blichert-Toft and Albarède, 1997) would not change our epsilon-values (identical within analytical error).

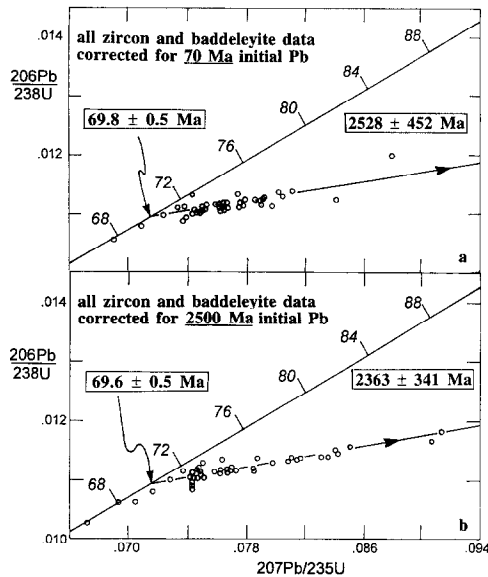


Fig. 7. Concordia diagrams compiling all U–Pb analyses, corrected for (a) 70 Ma, (b) 2500 Ma initial mantle Pb. For better distinction error ellipses are not shown. Note that intercept ages of both models are identical within analytical uncertainty, with the 2500 Ma model enhancing the influence of inheritance.

megacryst, and the upper intercept age is due to inheritance of old relic radiogenic Pb from high- μ minerals, present in the mantle prior to kimberlite genesis.

8.2. Model A

This model would require that all fragments suffered the same large degree of Pb-loss in very recent times. This scenario is in conflict with the very different U contents of zircon and baddeleyite (Table 2), for which large differences in degrees of episodic Pb-loss have to be expected. Such differential behaviour has been established by dating of zircon and baddeleyite from a single rock sample, showing very different degrees of episodic Pb-loss (e.g., Heaman and LeCheminant, 1993). Another argument against Model A is the absence of any evidence in favour of a major event in latest Miocene or Quaternary times. To cause such strong recent Pb-loss of late Palaeozoic–Mesozoic zircons, this event must have occurred at high temperatures ($> 600^{\circ}\text{C}$), i.e., it would correspond to kimberlite emplacement itself. However, there is no argument to make the kimberlite thermal event so recent.

8.3. Model B

This model assumes primary megacryst formation at 2.5 Ga followed by the kimberlite event at 70 Ma, to produce almost total Pb-loss in the old zircon and baddeleyite. In consequence, initial Pb has to be performed with such old common Pb producing the pattern shown in Fig. 7b. Initial Pb compositions used are: $\alpha = 14.03$, $\beta = 14.83$, and $\gamma = 33.72$ corresponding to a 2.5 Ga old model-mantle (Zartman and Doe, 1981). An important observation is that the resulting zircon–baddeleyite regression line yields concordia intercept ages that are identical with those obtained by correction with 70 Ma mantle Pb (69.8 ± 0.5 vs. 69.6 ± 0.5 Ma, and 2528 ± 452 vs. 2363 ± 341 Ma), despite their very different isotopic compositions ($^{207}\text{Pb}/^{206}\text{Pb}$: 1.057 for 2.5 Ga vs. 0.8590 for 70 Ma). Included in the regression calculation are three analyses of zircon-II that yield much older $^{207}\text{Pb}/^{206}\text{Pb}$ ages of 780, 820, 960 Ma (not shown in Fig. 7b). The major difference between the two patterns is stretching of the discordancy pattern, enhancing the influence of inherited components for 2.5 Ga old initial Pb.

Model B requires that both minerals lost more than 90% of their Pb at 70 Ma. Taking into account the measured Pb concentrations (Fig. 6), 2.5 Ga old zircon and baddeleyite would have lost between 5 and 1000 ppm of both radiogenic and initial Pb. Since such high levels of initial Pb are unrealistic, diffusion of exclusively radiogenic Pb had to be assumed, which is unlikely given the homogeneity of the grains and the absence of other mineral inclusions. Only highly metamict zircons are in principle susceptible to experience such strong loss and moreover, if kept at high temperatures, radiation damage would be self-annealing, with the zircon escaping metamictization. A further argument against very strong diffusional Pb-loss is the preservation of a ≈ 528 Ma U–Pb age in zircon, included in a Mbuji-Mayi diamond (Kinny et al., 1989).

If the primary age of the megacrysts was 2.5 Ga, the megacrysts would have formed in a reservoir having initial ε^{Hf} of +63 to +68. Such high values would be due to the very early strong LILE-depletion of mantle domains, with the depletion event occurring before megacryst formation at 2.5 Ga; however, no such Hf isotope evidence has yet been

discovered in favour of such strong early mantle depletion (Corfu and Noble, 1992; Vervoort et al., 1996).

8.4. Model C

This model assumes that 70 Ma old baddeleyite and zircon include small amounts of 2.5 Ga radiogenic Pb. As shown by the data (Table 2; Figs. 4 and 5), this Pb component is homogeneously distributed, and there is no correlation either with U, initial Pb or location of the fragments within the megacrysts. No relict cores were identified. For zircon, excess radiogenic Pb is less than 0.1 ppm and lies largely within the range of concentrations for common Pb. The same is true for all baddeleyites, because excess amounts of radiogenic Pb (1–2 ppm) lie well below the maximum amount of measured common Pb (4 ppm). The simultaneous incorporation of relict radiogenic and initial common Pb on the 1 ppm level would therefore be an excellent explanation for both the inherited component and the small degree of observed reverse discordancy. This means that inheritance is governed and buffered by the capacity of zircon and baddeleyite to integrate Pb in their crystal lattice during crystallization or re-crystallization.

To explain the presence of old radiogenic Pb components, different possibilities need to be examined. One possibility is that very old, roughly 2.5 Ga old zircon and baddeleyite underwent total re-crystallization at 70 Ma, expelling the bulk of their accumulated radiogenic Pb in the process. The absence of pronounced zoning in zircon or baddeleyite (Fig. 2) may be an argument that the megacrysts underwent such a process.

Another possibility is that the zircon and baddeleyite formed entirely new at 70 Ma. In this case, initial Pb at the 1 ppm level is the carrier of the excess radiogenic component. In order to evaluate this possibility we have corrected all our data for the most radiogenic types of 'common' Pb determined in: (1) kimberlite nodules at Mbuji-Mayi (Weis and Demaiffe, 1985), (2) East African carbonatites and lherzolite xenoliths (Lancelot and Allègre, 1974; Cohen et al., 1984), and (3) Pb metasomatic assemblages in peridotite xenoliths in Pacific oceanic islands (Hauri et al., 1993). These compositions correspond also to a HIMU component (Zindler and Hart,

1986), which has Nd and Sr isotopic compositions similar to those measured for the Mbuji-Mayi kimberlites (Demaiffe and Fieremans, 1981; Fieremans et al., 1984; Weis and Demaiffe, 1985). However, when applied to our data, none of the HIMU Pb compositions is able to produce our excess radiogenic components. On the other hand, HIMU corrections reduce the spread of discordancy among the megacrysts, suggesting that they have grain-specific initial Pb compositions. This interpretation is compatible with the observed differences in initial Hf isotope ratios (+5 to +10).

8.5. Other parameters

We have also examined the possibility that discordancy may be caused by isotopic disequilibrium. Such disequilibrium is potentially caused by the intermediate isotope ^{230}Th , which is enriched or depleted relative to secular equilibrium, dependent on fractionation of U and Th between crystallizing mineral and matrix. Isotopic disequilibrium ultimately leads to too old or too young $^{206}\text{Pb}/^{238}\text{U}$ -ages (Schärer, 1984). Using a Th/U = 4 for the mantle source, a crystallization age of 70 Ma, and Th/U calculated from radiogenic $^{208}\text{Pb}/^{206}\text{Pb}$ in Table 2, correction shows such disequilibrium to lie within the analytical uncertainties of our data ($\leq 0.1\%$ of $^{207}\text{Pb}/^{206}\text{Pb}$) and therefore, it cannot explain the discordancies observed. A second possibility for initial disequilibrium is Pa fractionation in the ^{235}U – ^{207}Pb decay chain to produce excess ^{207}Pb from ^{231}Pa . Given (1) the absence of expected differences in discordancy between zircon and baddeleyite, (2) the general knowledge of Th–U–Pa fractionation (e.g., Bacon and Rosholt, 1982), and (3) the ionic radius of these elements (M^{4+} of Th: 0.95; U: 0.97; Pa: 0.98 Å), this latter hypothesis (^{231}Pa) should be ruled out.

9. Origin of megacrysts and mantle processes

9.1. The megacrysts

Clues on the origin of the megacrysts are provided by their high Zr/Hf ratios, structural characteristics, and Pb–Hf isotope signatures. Since Zr is

very difficult to separate from Hf, due to similar sizes of their M^{4+} ions, extreme fractionation mechanisms are required. Normal melting of MORB sources does not fractionate Zr from Hf to such a large extent and our Zr/Hf ratios of 58 and 65 in zircon lie far from values of primitive mantle, N-MORBs or crustal zircons (Zr/Hf: 32–36). Equally high Zr/Hf ratios have been observed in zircons from intraplate alkali basalts and carbonatites (Zr/Hf: 52 and 81; Heaman et al., 1990), suggesting a genetic relationship between such strongly fractionated mantle and carbonatite genesis. A similar conclusion was drawn from high Zr/Hf observed in whole-rock samples of the Nyiragongo nephelinite (Zr/Hf \approx 80; Dupuy et al., 1992), other carbonatites, and metasomatized mantle xenoliths (Dupuy et al., 1992; Rudnick et al., 1993; Ionov et al., 1994). Metasomatism is an important factor in kimberlite genesis, and for the Mbuji-Mayi case, baddeleyite-coating observed on some of the zircon megacrysts yields direct evidence for its occurrence. Very small degrees of mantle melting in association with carbonatite genesis and mantle metasomatism therefore seems to be the most appropriate mechanism to generate the megacryst source material. This does not necessarily mean that the crystals formed directly from a magmatic liquid: the zircon and baddeleyite megacrysts may have grown through subsolidus reactions, caused by a thermal event that post-dates low-degree (high Zr/Hf) melting. In such a case, the inherited Pb components may be explained by the incorporation of very small amounts of material that carried 2.5 Ga old zircon and baddeleyite. These components may have been brought into the kimberlite source region by subduction of differentiated rocks, possibly oceanic crust (+traces of sediments?). This interpretation would be in agreement with the fact that (1) inclusions in Mbuji-Mayi diamonds are dominantly eclogitic in nature and (2) eclogite nodules are very abundant in the kimberlite.

9.2. Hf isotope signatures

ϵ_i^{Hf} calculated for 70 Ma old zircon and baddeleyite are listed in Table 3. The two zircon megacrysts yield initial signatures that are indistinguishable from each other (+8.1 and +8.4), whereas the baddeleyites show significant differences (+5.1, +6.0,

+6.2, +6.5, +10.2). The values show that the megacrysts originate from mantle domains which have experienced different time-integrated Lu–Hf fractionation histories. All $\epsilon_{70 \text{ Ma}}^{\text{Hf}}$ lie in the range expected for moderately to strongly depleted mantle reservoirs of Cretaceous age. Expressed in another way, Hf isotope signatures can be translated into initial Nd isotope signatures because Hf is roughly twice as much fractionated from Lu than Nd from Sm, in the case of 15–20% lherzolite melting ($\epsilon^{\text{Hf}} \approx 2\epsilon^{\text{Nd}}$; e.g., Patchett, 1983; Vervoort et al., 1996). Our values correspond to $\epsilon_{70 \text{ Ma}}^{\text{Nd}}$ of +2.5 to +5, lying in the range of those measured in phenocrysts of the Mbuji-Mayi kimberlites (+2 and +6; Demaiffe and Fieremans, 1981; Fieremans et al., 1984; Weis and Demaiffe, 1985).

These data could alternatively reflect: (1) mantle sources depleted to various degrees by different degrees of early (Precambrian) melt extraction; (2) homogeneously depleted mantle domains that were affected by different degrees of secondary enrichment; (3) a combination of (1) and (2).

10. Summary and conclusions

(1) U–Pb analyses of zircon and baddeleyite megacrysts from the Mbuji-Mayi kimberlite yield concordia intercept ages of 69.8 ± 0.5 (2σ) and about 2528 Ma. The \approx 70 Ma age can be interpreted as the time of megacrysts formation in the mantle, and the Precambrian age likely arises from the incorporation of inherited radiogenic Pb, present in the subcontinental mantle at the time of kimberlite formation.

(2) Very small degrees of mantle melting seems to be the most appropriate mechanism to generate high Zr/Hf in the megacrysts, possibly in combination with carbonatite genesis and mantle metasomatism. The zircon and baddeleyite megacrysts may have formed either directly from a magma, by metasomatism, or through subsolidus crystallization.

(3) The zircon and baddeleyite megacrysts have $\epsilon_{70 \text{ Ma}}^{\text{Hf}}$ ranging from +5 to +10 substantiating megacryst extraction from mantle reservoirs showing significantly different time-integrated Lu–Hf fractionation histories. The variable Hf signatures may partially be produced by secondary enrichment of

strongly depleted mantle. Observed crystallographic complexities of Mbuji-Mayi diamonds and variations in their $\delta^{15}\text{N}$ and $\delta^{13}\text{C}$ (Javoy et al., 1984) may have identical explanations.

(4) The most plausible scenario for the genesis of the Mbuji-Mayi kimberlite is successive melting of variously differentiated superposed mantle domains, with a stepwise migration of magmas to the surface. Residence times of the evolving magmas must be long enough to allow extraction of megacrysts and diamonds from the solid mantle, followed by partial resorption and re-crystallization of the xenocrysts in the kimberlite magma.

Acknowledgements

We thank C. Fieremans for access to the megacrysts and helpful discussion of the Mbuji-Mayi geology. We are indebted to E. Lesure for drafting the figures, and we thank S. Gilder, J. Vervoort and two anonymous colleagues for critical reading, very careful reviewing, and constructive comments. This is IPG–Paris contribution No. 1485.

References

- Bacon, M.P., Rosholt, J.N., 1982. Accumulation rates of ^{203}Th , ^{231}Pa , and some transition metals on the Bermuda Rise. *Geochim. Cosmochim. Acta* 46, 651–666.
- Blichert-Toft, J., Albarède, F., 1997. The Lu–Hf isotope geochemistry of chondrites and the evolution of the mantle–crust system. *Earth Planet. Sci. Lett.* 148, 243–258.
- Cohen, R.S., O’Nions, R.K., Dawson, J.B., 1984. Isotope geochemistry of xenoliths from East Africa: implications for development of mantle reservoirs and their interaction. *Earth Planet. Sci. Lett.* 68, 209–220.
- Corfu, F., Noble, S.R., 1992. Genesis of the southern Abitibi greenstone belt, Superior Province, Canada: evidence from zircon Hf isotope analyses using a single filament technique. *Geochim. Cosmochim. Acta* 56, 2081–2097.
- Davis, G.L., 1977. The ages and U contents of zircons from kimberlites and associated rocks. Extended Abstr., 2nd Int. Kimberlite Conf., Santa Fe, N.M. (abstr.).
- Delhal, J., Ledent, D., Pasteels, P., 1975. L’âge du complexe granitique et migmatitique de Dibaya (région du Kasai, Zaire) par les méthodes Rb–Sr et U–Pb. *Ann. Soc. Géol. Belg.* 98, 141–154.
- Demaiffe, D., Fieremans, M., 1981. Strontium-isotopic geochemistry of the Mbuji-Mayi and Kundelungu kimberlites (Zaire, Central Africa). *Chem. Geol.* 31, 311–323.
- Demaiffe, D., Fieremans, M., Fieremans, C., 1991. The kimberlites of Central Africa; a review. In: Kampunzu, A.B., Lubala, R.T. (Eds.), *Magmatism in Extensional Structural Settings*. Springer-Verlag, Berlin, pp. 537–559.
- Dupuy, C., Liotard, J.M., Dostal, J., 1992. Zr/Hf fractionation in intraplate basaltic rocks: carbonate metasomatism in the mantle source. *Geochim. Cosmochim. Acta* 56, 2417–2423.
- Elfadili, S., Demaiffe, D., André, L., 1995. Origin of eclogite nodules from the Mbuji-Mayi kimberlites (Kasi, Zaire): subducted ancient oceanic crust? 6th Int. Kimberlite Conf., Novosibirsk, pp. 146–148.
- Fieremans, C., 1977. Mode of occurrence and tectonic control of the kimberlite bodies in East Kasai (Zaire). 2nd Int. Kimberlite Conf., Santa Fe (abstr.).
- Fieremans, M., Ottenburgs, R., 1979a. Kimberlite inclusions and chlorite nodules from the kimberlite breccia of Mbuji-Mayi (Eastern Kasai) Zaire. *Bull. Soc. Belg. Géol.* 88, 205–224.
- Fieremans, M., Ottenburgs, R., 1979b. The occurrence of zircon and baddeleyite crystals in the kimberlite formation at Mbuji-Mayi (Bakwanga, Zaire). *Bull. Soc. Belg. Géol.* 88, 25–31.
- Fieremans, M., Hertogen, J., Demaiffe, D., 1984. Petrography, geochemistry and strontium isotopic composition of the Mbuji-Mayi and Kundelungu kimberlites (Zaire). In: Kornprobst, J. (Ed.), *Kimberlites and Related Rocks*. Elsevier, Amsterdam, pp. 107–120.
- Hauri, E.K., Shimizu, N., Dieu, J.J., Hart, S.R., 1993. Evidence for hot-spot-related carbonatite metasomatism in the oceanic upper mantle. *Nature* 365, 221–227.
- Heaman, L.M., LeCheminant, A.N., 1993. Paragenesis and U–Pb systematics of baddeleyite (ZrO_2). *Chem. Geol.* 110, 95–126.
- Heaman, L.M., Bowins, R., Crocket, J., 1990. The chemical composition of igneous zircon suites: implications for geochemical tracer studies. *Geochim. Cosmochim. Acta* 54, 1597–1607.
- Ionov, D.A., Hofmann, A.W., Shimizu, N., 1994. Metasomatism-induced melting in mantle xenoliths from Mongolia. *J. Petrol.* 35, 753–785.
- Ito, E., White, W.M., Göpel, C., 1988. The O, Sr, Nd and Pb isotopic geochemistry of MORB. *Chem. Geol.* 62, 157–176.
- Jaffey, A.H., Flynn, K.F., Glendenin, L.E., Bentley, W.C., Essling, A.M., 1971. Precision measurements of half-lives and specific activities of ^{235}U and ^{238}U . *Phys. Rev. C* 4, 1889–1906.
- Javoy, M., Pineau, F., Demaiffe, D., 1984. Nitrogen and carbon isotopic composition in the diamonds of Mbuji-Mayi (Zaire). *Earth Planet. Sci. Lett.* 68, 399–412.
- Jochum, K.P., Seufert, H.M., Spettel, B., Palme, H., 1986. The solar-system abundances of Nb, Ta, and Y, and the relative abundances of refractory lithophile elements in differentiated planetary bodies. *Geochim. Cosmochim. Acta* 50, 1173–1183.
- Kinny, P.D., Compston, W., Bristow, J.W., Williams, I.S., 1989. Archaean mantle xenocrysts in a Permian kimberlite: two generations of kimberlitic zircon in Jwaneng DK2, southern Botswana. In: Ross, J. (Ed.), *Kimberlites and Related Rocks*. *Geol. Soc. Aust. Spec. Publ.* 14, 833–842.
- Kinny, P.D., Meyer, H.O.A., 1994. Zircons from the mantle: a new way to date old diamonds. *J. Geol.* 102, 475–481.

- Kresten, P., Fels, P., Berggren, G., 1975. Kimberlitic zircon—a possible aid in prospecting for kimberlites. *Miner. Deposita* 10, 47–56.
- Krogh, T.E., 1973. A low-contamination method for hydrothermal decomposition of zircon and extraction of U and Pb for isotopic age determinations. *Geochim. Cosmochim. Acta* 37, 485–494.
- Krogh, T.E., 1982. Improved accuracy of U–Pb zircon ages by creation of more concordant systems using air abrasion technique. *Geochim. Cosmochim. Acta* 46, 637–649.
- Kudoh, Y., Prewitt, C.W., Arashi, A., 1989. Premonitory twinning in the high-pressure phase transition of ZrO_2 . *Carnegie Inst. Washington, Yearb.* 88, 108–110.
- Lancelot, J.R., Allègre, J.C., 1974. Origin of carbonatitic magma in the light of the U–Pb–Th isotope system. *Earth Planet. Sci. Lett.* 22, 233–238.
- Murali, A.V., Parthasarathy, R., Mahadevan, T.M., Sankar Das, M., 1983. Trace element characteristics, REE patterns and partition coefficients of zircons from different geological environments—case study on Indian zircons. *Geochim. Cosmochim. Acta* 1983, 2047–2052.
- Mvuemba, N.F., 1980. *Minéralogie des mégacrists, des xénolithes écolitiques et granulitiques et des inclusions cristallines dans les diamants de la kimberlite du Kasai, Zaïre.* Thèse Doct., Université de Louvain, 221 pp.
- Nixon, P.H., Boyd, F.R., 1973. The discrete nodule association in kimberlites from northern Lesotho. In: Nixon, P.H. (Ed.), *Lesotho Kimberlites*. Lesotho National Development Corporation, Maseru, pp. 67–75.
- Ottenburgs, R., Fieremans, M., 1979. Rutile–silicate intergrowth from the kimberlite formation at Mbuji-Mayi (Bakwonga, Zaïre). *Bull. Soc. Belg. Géol.* 88, 197–203.
- Patchett, P.J., 1983. Importance of Lu–Hf isotopic system in studies of planetary chronology and chemical evolution. *Geochim. Cosmochim. Acta* 47, 81–91.
- Patchett, P.J., Tatsumoto, M., 1980. A routine high-precision method for Lu–Hf isotope geochemistry and chronology. *Contrib. Mineral. Petrol.* 75, 263–267.
- Rudnick, R.L., McDonough, W.F., Chappell, B.W., 1993. Carbonatite metasomatism in the northern Tanzanian mantle: petrographic and geochemical characteristics. *Earth Planet. Sci. Lett.* 114, 463–475.
- Scatena-Wachel, D.E., Jones, A.P., 1984. Primary baddeleyite (ZrO_2) in kimberlite from Benfontein, South Africa. *Miner. Mag.* 48, 257–261.
- Schärer, U., 1984. The effect of initial ^{230}Th disequilibrium on young U–Pb ages: the Makalu case, Himalaya. *Earth Planet. Sci. Lett.* 67, 191–204.
- Schärer, U., Gower, C.F., 1988. Crustal evolution in eastern Labrador: constraints from precise U–Pb ages. *Precambrian Res.* 38, 405–421.
- Steiger, R.H., Jäger, E., 1977. Subcommittee on geochronology: convention on the use of decay constants in geo- and cosmochronology. *Earth Planet. Sci. Lett.* 36, 359–362.
- Stöffler, D., Langenhorst, F., 1994. Shock metamorphism of quartz in nature and experiment, I. Basic observation and theory. *Meteoritics* 29, 155–181.
- Vervoort, J.D., Patchett, P.J., Gehrels, G.E., Nutman, A.P., 1996. Constraints on early Earth differentiation from hafnium and neodymium isotopes. *Nature* 379, 624–627.
- Weis, D., Demaiffe, D., 1985. A depleted mantle source for kimberlites from Zaïre: Nd, Sr and Pb isotopic evidence. *Earth Planet. Sci. Lett.* 73, 269–277.
- Zartman, R.E., Doe, B.R., 1981. Plumbotectonics—the model. *Tectonophysics* 75, 135–162.
- Zindler, A., Hart, S., 1986. Chemical geodynamics. *Ann. Rev. Earth Sci.* 14, 493–571.